Published in final edited form as:
J Magn Reson Imaging. 2011 October ; 34(4): 791–798. doi:10.1002/jmri.22687.

Cortical Calcification in Sturge-Weber Syndrome on MRI-SWI: Relation to Brain Perfusion Status and Seizure Severity

Jianlin Wu, MD, PhD[1,2], **Bisher Tarabishy, MD**[2], **Jiani Hu, PhD**[2], **Yanwei Miao, MD**[2,3], **Zhaocheng Cai, MS**[3], **Yang Xuan, BS**[2], **Michael Behen, PhD**[4], **Meng Li, MS**[2], **Yongquan Ye, PhD**[2], **Richard Shoskey, BS**[2], **E. Mark Haacke, PhD**[2], and **Csaba Juhász, MD, PhD**[4]

[1] Zhongshan Hospital of Dalian University, Department of Radiology Dalian, Liaoning

[2] Department of Radiology, Wayne State University, 3990 John R Road, Detroit, MI 48202, USA

[3] Department of Radiology, the First Affiliated Hospital, Dalian Medical University, 222 Zhongshan Road, Dalian, Liaoning 116011, China

[4] Departments of Pediatrics and Neurology, Wayne State University, Children's Hospital of Michigan, 3901 Beaubien Blvd., Detroit, MI 48201, USA

Abstract

Purpose—To determine the relationship between calcified cortex and perfusion status of white matter and seizure severity in patients with Sturge-Weber Syndrome (SWS), a sporadic neuro-cutaneous disorder characterized by a leptomeningeal angioma, progressive brain ischemia and a high incidence of seizures, using Susceptibility Weighted Imaging (SWI) and Dynamic Susceptibility Contrast-enhanced Perfusion Weighted Imaging (DSC-PWI).

Materials and Methods—Fifteen children (ages: 0.9-10 years) with unilateral SWS prospectively underwent MR imaging. The degree of cortical calcification was assessed using SWI while perfusion status was quantified using DSC-PWI images (asymmetries of various perfusion parameters). Comparisons between calcification, perfusion status and seizure variables were performed.

Results—Patients with severely calcified cortex demonstrated significantly lower perfusion in the ipsilateral white matter (mean asymmetry: −0.52±0.22) as compared to patients with only mildly calcified cortex or no calcification (mean asymmetry: 0.08±0.25). Patients with severely calcified cortex also suffered from a higher seizure burden (a composite measure of seizure frequency and epilepsy duration; p=0.01) and a trend for earlier seizure onset and longer epilepsy duration.

Conclusion—Severe calcification in the affected hemisphere is related to severely decreased perfusion in underlying white matter and is associated with more severe epilepsy in SWS patients.

Keywords

Sturge-Weber Syndrome; PWI; Epilepsy; Calcification

Introduction

Sturge-Weber syndrome (SWS) is a non-hereditary phakomatosis classically characterized by a facial port-wine stain in the trigeminal nerve distribution, an ipsilateral parieto-occipital

Corresponding Author and Reprint Info: Dr. Csaba Juhász, Departments of Pediatrics and Neurology, Wayne State University, Children's Hospital of Michigan, 3901 Beaubien Blvd., Detroit, MI 48201, USA.

leptomeningeal angioma, and glaucoma (1). Clinically, patients with SWS demonstrate a highly variable course with many patients exhibiting few if any motor deficits and near normal cognitive function while other patients suffer from severe hemiparesis and developmental delay (2, 3). Seizures typically begin in early childhood and may worsen with age. They are often accompanied by stroke-like episodes where patients develop hemiparesis contralateral to the leptomeningeal angioma (4).

It is thought that the leptomeningeal angioma results from failure of the primitive cephalic venous plexus to regress. As a result, normal, superficial cortical venous drainage is absent and is replaced by the leptomeningeal angioma (1). The lack of a normal cortical venous drainage system results in venous hypertension and chronic ischemia with subsequent brain atrophy in the affected cortex (5). Prolonged seizures are thought to worsen the underlying ischemia by increasing metabolic demand in an area of the brain where little, if any, flow reserve is present (6). The vessels of the leptomeningeal angioma also appear prone to thrombosis contributing to cortical ischemia (7). Calcification of the atrophic cortex is a well-described pathologic feature of SWS and is thought to result from a combination of gliosis in ischemic cortex and abnormal vessels (1, 8).

The imaging findings of SWS on CT and MRI include atrophy of the involved cortex, pial enhancement, prominent transmedullary veins, enlarged choroid plexus and calcification of the cortex (9, 10). The development of these findings follows a temporal progression with the involved brain parenchyma often appearing normal in the neonatal period. Susceptibility Weighted Imaging (SWI) is more accurate in identifying the presence of and quantifying the degree of calcification in the affected cortex than conventional MRI sequences (11).

Impaired venous drainage in brain tissue underlying the leptomeningeal angioma leads to abnormal perfusion, the main cause of progressive pathologic changes and tissue damage in SWS. Therefore, direct measure of brain tissue perfusion may be helpful in evaluating severity of brain involvement in affected patients, particularly before the more classically described pathologic and structural imaging changes of SWS have occurred. Previous studies quantified cerebral blood flow abnormalities in children with SWS using single photon emission tomography (SPECT) (12). However, this technique yields low-resolution images, lacks absolute quantification and involves radiation exposure to the patients.

Dynamic Susceptibility Contrast-enhanced Perfusion Weighted Imaging (DSC-PWI), an MRI technique that measures relative perfusion parameters in the brain (13), offers distinct advantages over nuclear medicine techniques. Briefly, DSC-PWI assesses changes in signal intensity over time in a given voxel after the administration of a gadolinium based contrast agent, exploiting the paramagnetic properties of gadolinium. DSC-PWI's main advantage over nuclear medicine perfusion techniques is the lack of radiation exposure and its ability to correlate perfusion abnormalities with detailed anatomic images. Compared to Arterial Spin Labeling (ASL), an emerging alternative MRI perfusion technique, DSC-PWI produces a more robust signal-to-noise ratio, a particular advantage in white matter perfusion measurements.

In this study, we sought to link findings on high-resolution PWI with cortical calcifications. We also studied if severity of calcification is related to severity of clinical seizures

Materials and Methods

Patient Selection

Fifteen children with SWS were prospectively recruited for this study between December of 2006 and March of 2009. Inclusion criteria were (1) a prior diagnosis of SWS with unilateral

brain involvement based on clinical and imaging features; (2) an age range between 6 months and 10 years; (3) availability of good quality SWI and DSC-PWI images. Patients were excluded if they had bilateral hemispheric disease since an unaffected hemisphere must be present in order to make a meaningful comparison between sides on DSC-PWI.

All imaging studies were performed in compliance with regulations of the institutional review board and written informed consent of the parent or legal guardian was obtained.

Clinical Seizure Variables.

All but one patient had a history of seizures. To analyze if seizures were related to severity of calcification (see below), the following seizure variables were analyzed, based on information provided by medical records and parent interviews: 1. Age at seizure onset (in years); 2. Duration of epilepsy (time between age at seizure onset and MRI scan analyzed); 3. Seizure frequency. Since seizure frequency is difficult to determine with exact accuracy in children with SWS, a seizure frequency score was calculated based on a scoring system proposed by Engel et al (14). The original 12-point scoring system was proposed for evaluating seizure frequency after epilepsy surgery. We used a modified 7-point scale (0–6), better suited for our patient population, since some of the categories described by Engel et al simply did not apply in our patients. Our scale was as follows: 0: no seizures at all; 1: <1 seizure per year; 2: 1 seizure seizures per year, in average; 3: 2-11 seizure(s) per year; 4: 1–3 seizure(s) per month; 5: 1–6 seizures per week; 6:≥1 seizure(s) per day. 4. Finally, to characterize the life-time seizure burden, a “seizure burden score” was also calculated by multiplying the duration of epilepsy by the seizure frequency score. All seizure variables are detailed in table 1.

MR Imaging

All children underwent MRI examination on a Sonata 1.5 T MR scanner (Siemens, Erlangen, Germany) with a standard head coil. Before MR examination, patients younger than 7 years old were sedated with pentobarbital (3 mg/kg) followed by fentanyl (1μg/kg). The protocol included an axial 3D T1-weighted gradient-echo acquisition (TR = 20 ms; TE = 5.6 ms; flip angle = 25°; voxel size = 1×0.5×2 mm^3; FOV = 256mm × 192mm; Slices = 64; Section Thickness = 2 mm) , an axial T2-weighted turbo spin-echo acquisition (TR=5020 ms; TE=106 ms; voxel size=1×1×6 mm^3; FOV= 256mm × 192mm; Slices = 30; Section Thickness = 4 mm), a dynamic susceptibility contrast enhanced high resolution MR perfusion imaging acquisition, an axial velocity compensated 3D gradient echo SWI acquisition and a postgadolinium T1-weighted acquisition (imaging parameters were the same as the non-contrast T1 sequence mentioned above).

The DSC-PWI data was obtained using a two-dimensional, single-shot, gradient echo EPI sequence with an 8-channel head coil (TR = 2200 ms, TE = 98ms, flip angle = 60°, slice thickness = 4 mm). Parallel imaging was used with GRAPPA (generalized autocalibrating partially parallel acquisitions) and an acceleration factor of 2. The field of view (FOV) was 256 mm × 256 mm and the acquisition matrix size was 256 × 256 but was interpolated to 512 × 512 for display purposes. We acquired 50 dynamic phases with a temporal resolution of 3 seconds. The contrast agent gadolinium-DTPA (Magnevist, Berlex, USA) was bolus injected by a power injector (Medrad, Spectris MR injection system, USA) with a dose of 0.1 mmol/kg of body weight at a rate of 3 ml/sec. The smaller voxel size of 1 × 1 × 4 mm^3 compared to those published previously (14, 15) may improve the ability to observe subtle structures in cerebral parenchyma, hence the name high resolution DSC-PWI.

A 3D fully balanced gradient-echo turbo SWI sequence was performed with flip angle= 20°; TR, 89 ms; TE, 40 ms; acquisition matrix, 512×256×48; FOV, 256×256×96 mm; bandwidth, 160 Hz/pixel. Both magnitude and phase images were saved.

SWI Analysis

Both magnitude and phase images were used to create final SWI images. SWI "filtered" phase images were used to estimate the degree of calcification. Due to the diamagnetic properties of calcium, the calcified tissues showed increased signal in the "filtered" phase images and were easy to distinguish. It has been previously demonstrated that phase images provide identification of calcified regions comparable to CT in both brain and peripheral vessels (17,18). Two neuroradiologists detected the location of cortical calcification in a blinded fashion and further determined the score of calcification according to the following criteria: A score of 0 was assigned to cortex that had normal signal and therefore was likely not calcified. A score of 1 was assigned to cortex that had punctate foci of increased signal suggestive of early calcification. Finally, a score of 2 was assigned to cortex with linear areas of increased signal indicating linear cortical calcifications. Figure 1 gives examples of each grade of calcification. If multiple lobes showed cortical calcification in the same case, the highest score in all affected lobes was recorded as the final value. The scores were compared between the two observers.

PWI analysis

Relative Cerebral Blood Flow (rCBF), relative Mean Transit Time (rMTT), and relative Cerebral Blood Volume (CBV) maps were derived from the perfusion data using software developed in-house (Signal process in neuroradiology, SPIN). To create perfusion maps, deconvolution with singular value decomposition (SVD) was used to create quantitative maps of rCBF, rCBV and MTT (19, 20). The position of the arterial input function (AIF) was automatically determined by using the maximum concentration (Cmax), time to peak (TTP) and first moment MTT (fMTT). The concentration-time curve for arteries has short fMTT, short TTP and high Cmax. Twenty voxels, which best fit these properties were selected. Then the concentration-time curves of these voxels were averaged, smoothed and truncated to avoid the second pass of the tracer. rCBF, rCBV and MTT values in the white matter ipsilateral to the angioma and in contralateral homotopic white matter were manually measured by two neuroradiologists. White matter, rather than cortex, was analyzed in this study, as selective and accurate measurement of cortical perfusion would be difficult in children with SWS due to the confounding effect of the low-flow leptomeningeal angioma directly overlaying affected cortical regions, as well as artifact from cortical calcification. Affected white matter was defined as the presence of abnormally enhancing vessels or the presence of a leptomeningeal venous angioma overlying the cortical surface. Two to three regions of interest (ROIs; size: 20–40 pixels) were placed on every slice with an apparent vessel abnormality in the affected and contralateral white matter (2–8 slices in individual patients, depending on the extent of vessel abnormality; mean: 4.5 slices), as seen in figure 2. An effort was made to avoid placing the ROIs over vessels, cortex and ventricle. ROI placement was performed using the CBF map, a map which shades the vessels and cortex with a red and green scale while the white matter is shaded blue, allowing for accurate placement of ROIs solely in white matter. If cortical calcification was seen in the affected lobe, ROIs were set in the WM in the same lobe. Furthermore, all parameters were measured slice by slice, covering all affected regions. The final CBF values quoted for each patient were the mean of measurements in all slices of affected cortex.

Statistical Analysis

Intraobserver and interobserver reliability was first investigated with a target of greater than 90% after the rCBF, rCBV, and MTT values had been measured twice by two

neuroradiologists for all subjects. Reliability was investigated using the Intraclass Correlation Coefficient.

Asymmetry indices (AIs) for all three PWI variables were calculated as follows:

$$AI=(I - C)/[(I+C)/2]$$

Where C and I represent rCBF values calculated for white matter ipsilateral (I) and contralateral (C) to the affected hemisphere. Negative AI values indicated lower perfusion values on the ipsilateral side. We tested if perfusion variables (CBF, CBV and MTT measured ipsi- and contralateral to the angioma, as well as CBF, CBV and MTT AI values) were different among patients with different calcification scores using ANOVA, followed by pair-wise post-hoc comparisons. In the second step, clinical variables (age and seizure variables) were compared among calcification groups to determine if there was a relation between severity of calcification and seizure severity. We used the non-parametric Mann-Whitney U-test in this latter comparison due to the non-normal distribution of some of the seizure variables. All statistical analyses were performed using SPSS statistics for Windows (Release 16.0; SPSS, Chicago, IL). All statistics was performed with a 0.05 level of significance.

Results

Intra- and inter-observer correlation coefficients of rCBF, rCBV and MTT were all over 0.90 (0.95, 0.94 and 0.97 respectively for rCBF, rCBV and MTT). The inter-observer reliability of calcification scores was 100%.

In all, 7 cases showed punctuate or string-like high-intensity lesions in “filtered” phase images, indicating cortical calcification in the lobe(s) affected by the leptomeningeal angioma. The location and scores of calcification are seen in table 1. Calcification groups (scores 0–2) showed an overall difference for all three PWI asymmetry variables ($p<0.01$ for all AIs). Posthoc comparisons showed significant differences between the “no calcification”/”mild calcification” vs. “severe calcification” subgroups with respect to all three PWI variables (rCBF AI: p=0.001 [score 0 vs. 2], p=0.015 [score 1 vs. 2]; rCBV AI: p=0.002; p=0.04; MTT AI: p=0.002. p=0.03). All patients with severe calcification (score 2) had CBF AI values below −0.27 (mean CBF AI: -0.52±0.22), indicating a greater than 27% decrease in blood flow on the side of the angioma. In contrast, all patients with no or mild calcification (scores 0 and 1) had CBF AI values above −0.22 (mean: 0.08±0.25), indicating a less than 22% decrease in blood flow on the angioma side, including 5 patients who actually had higher CBF values on the angioma side (table 1). Values in the two cases with “punctate calcifications” (score 1) were similar to those with “no calcification” (score 0) for all perfusion variables ($p>0.7$). Therefore, patients with no and mild calcifications were combined (n=10), and their clinical variables were compared to those with severe calcification (score 2, n=5). This comparison showed that patients with severe calcification had higher seizure burden scores than those with no or mild calcification (18.3±19.0 vs. 3.7±4.7, respectively; p=0.01); this group also showed a trend for earlier seizure onset (mean: 0.4±0.3 vs. 1.9±1.8 years, respectively; p=0.09) and longer seizure duration (mean: 4. 7±3.5 years vs. 2.1±2.6 years; p=0.075). Age (p=0.42) and seizure frequency scores (p=0.16) were not different between these two calcification groups.

Discussion

Because the clinical course of SWS is highly variable, deciding on the appropriate management can often be challenging. To date, conventional imaging findings on CT and

standard MRI sequences have been shown to become more conspicuous as the disease progresses, but they have not been found to be of significant prognostic value (21). The promise of functional imaging such as DSC-PWI and FDG-PET is that brain abnormalities that are not normally visible on conventional imaging may become so on functional imaging (22, 23).A recent study of seven children with SWS found that PWI was slightly better than conventional imaging at defining the territory of abnormality (23). Indeed, abnormalities were seen in the contralateral hemisphere of two patients when none was suspected on conventional MR imaging. A separate study of PWI in children with SWS found a correlation between the severity and extent of perfusion defect and the patient's motor symptoms (21).

Our present study demonstrates a link between a low perfusion state in the white matter (mean 52%±22% decrease of CBF, as compared to the unaffected hemisphere) and the presence of severe cortical calcifications. A similar link has been proposed in a prior case report of two SWS patients, where CT was used to detect calcification and perfusion abnormalities were studied by single photon emission tomography (24). Histologic studies have shown that calcification in SWS appears to be related to a combination of gliosis due to chronic anoxia and venous hypertension along with altered vascular permeability of the abnormal vessels overlying the involved cortex (1, 8). It has also been shown that the presence of such calcifications as detected on SWI corresponds to areas of severely hypometabolic cortex as determined on FDG-PET (5). Findings on perfusion imaging in SWS appear to be more sensitive in defining affected cortex than conventional imaging findings alone (23). Decreased venous outflow via abnormal or occluded cortical vessels impairs blood flow in subcortical white matter (which is is normally drained via these vessels), which can lead to the observed decreases of CBF and CBV values in the chronic stages of the disease. The presence of a low-perfusion state underlying the area of the leptomeningeal angioma may well predict the development of gliotic, calcified, and hypometabolic cortex, although our cross-sectional study does not establish a temporal relationship between these. However, our study does lend support to the notion that a chronic hypoxic state caused by inadequate venous drainage and venous hypertension likely contributes to the development of cortical calcification.

Most of our patients were scanned under sedation, using pentobarbital and fentanyl. Previous studies in rats have demonstrated uniformly decreased cerebral blood flow with the use of pentobarbital or fentanyl (25). Because of this, the potential effects of anesthetic agents on cerebral perfusion likely did not affect our results considerably, as we have used asymmetry (rather than absolute perfusion) values in our analyses. This approach is advantageous to diminish interindividual variations of brain perfusion due to age or drug effects.

It should be also noted that some patients, all with no or mild calcification on SWI, showed *increased* white matter perfusion in the affected hemisphere, as compared to the contralateral side (Table 1). The reason for these increases is not completely clear, but they may be related to transient increases of blood flow and glucose metabolism reported in some (mostly young) patients shortly before or after the onset of initial seizures (26, 12). The young age at seizure onset of such patients suggests that increased perfusion may represent an early stage of blood flow abnormalities, possibly related to ongoing hypoxic damage. A similar phenomenon has been described in infants with perinatal hypoxia, both on PWI and positron emission tomography (27, 28). It was speculated that transient hyperperfusion/ hypermetabolism may be due to hypoxia-induced glutamate release that may contribute to subsequent excitotoxic tissue damage.

In addition to a relation to brain perfusion status, our study also suggests that brain calcification may also be associated with severe, chronic seizures in children with SWS. This is consistent with previous data suggesting that the presence of calcification in the brain is more than simply an inert imaging finding and may in fact exert a deleterious effect on neuronal function (29). Calcium deposits appear to have an association with multiple neurologic symptoms including seizures and movement disorders. In neurocysticercosis, the most common cause of symptomatic seizures worldwide, the presence of calcium deposits has been linked with an increased incidence of seizures (30). A previous study also demonstrated a decrease in seizure frequency in two patients with calcifications on imaging after initiating therapy with disodium etidronate, a calcium chelating agent (29). Our findings raise the possibility that the calcifications seen in SWS may contribute to epileptogenesis and pharmacologic reversal of calcium deposits may be helpful in reducing seizure frequency. Also, since our data demonstrate that severe calcification occurs in the setting of significantly decreased brain perfusion (mean -52%±22%), PWI may be useful in identifying low perfusion areas that are prone to calcification, triggering frequent seizures, thereby identifying patients at risk and possible candidates for early treatment as well. This could be addressed in future, longitudinal studies.

In conclusion, our study demonstrates a link between severely diminished white matter perfusion, the presence of marked cortical calcification and a higher seizure burden in children with SWS. These findings lend further support to prevailing theories regarding the development of calcification in Sturge-Weber syndrome. They also provide an additional imaging tool that may prove useful to clinicians in evaluating the severity and extent of disease. Further research establishing a temporal relationship between perfusion findings, calcification and clinical progression may ultimately prove helpful in guiding treatment.

Acknowledgments

We are grateful to Yang Xuan BS for his technical support in the MRI acquisition. We also thank Majid Khalaf MD, Anne Deboard RN and Jane Cornett RN for their assistance in sedation. We thank the Sturge-Weber Foundation for referring patients to us. We are also grateful to the families and children who participated in the study.

Grant Support:

Contract grant sponsor: National Institutes of Health; Grant number: NS041922 (PI: Juhasz).

Contract grant sponsor: National Science Foundation of China; Grant number: 30870699 (PI: Wu).

References

1. Comi A. Topical Review: Pathophysiology of Sturge-Weber Syndrome. J Child Neurol. 2003; 18:509–516. [PubMed: 13677575]
2. Sujansky E, Conradi S. Outcome of Sturge-Weber syndrome in 53 adults. Am J Med Genet. 2005; 57:35–45. [PubMed: 7645596]
3. Sujansky E, Conradi S. Sturge-Weber Syndrome: Age of Onset of Seizures and Glaucoma and the Prognosis for Affected Children. J Child Neurol. 1995; 10:49–58. [PubMed: 7769179]
4. Roach ES, Riela AR, Chugani HT, Shinar S, Bodensteiner JB, Freeman J. Sturge-Weber Syndrome: Recommendations for Surgery. J Child Neurol. 1994; 9:190–192. [PubMed: 8006373]
5. Juhasz C, Haccke EM, Hu J, et al. Mutimodality Imaging of Cortical and White Matter Abnormalities in Sturge-Weber Syndrome. Am J Neuroradiol. 2007; 28:900–906. [PubMed: 17494666]
6. Aylett SE, Neville BGR, Cross JH, Boyd S, Chong WK, Kirkham FJ. Sturge-Weber syndrome: cerebral haemodynamics during seizure activity. Dev Med Child Neurol. 1999; 41:480–485. [PubMed: 10454232]

7. Garcia JC, Roach ES, McLean WT. Recurrent thrombotic deterioration in the Sturge-Weber syndrome. Childs Brain. 1981; 8:427–433. [PubMed: 7307643]
8. Prayson RA, Grewal ID, McMahon JT, Barna BP, Estes ML. Leukocyte Adhesion Molecules and X-Ray Energy Dispersive Spectroscopy in Sturge-Weber Disease. Pediatr Neurol. 1996; 15:332–336. [PubMed: 8972534]
9. Marti-Bonmati L, Menor F, Poyatos C, Cortina H. Diagnosis of Sturge-Weber Syndrome: Comparison of the Efficacy of CT and MR Imaging in 14 Cases. AJR. 1992; 158:867–871. [PubMed: 1546607]
10. Wasenko JJ, Rosenbloom SA, Duchesneau PM, Lanzieri CF, Weinstein MA. The Sturge-Weber syndrome: comparison of MR and CT characteristics. Am J Neuroradiol. 1990; 11:131–134. [PubMed: 2105594]
11. Hu J, Yu Y, Juhasz C, et al. MR Susceptibility weighted Imaging (SWI) Complements Conventional Contrast Enhanced T1 Weighted MRI in Characterizing Brain Abnormalities of Sturge-Weber Syndrome. J Magn Reson Imaging. 2008; 28:300–307. [PubMed: 18666142]
12. Pinton F, Chiron C, Enjolras O, Motte J, Syrota A, Dulac O. Early single photon emission computed tomography in Sturge-Weber syndrome. J Neurol Neurosurg Psychiatry. 1997; 63:616–621. [PubMed: 9408103]
13. Keston P, Murray AD, Jackson A. Cerebral Perfusion Imaging using Contrast-enhanced MRI. Clin Radiol. 2003; 58:505–513. [PubMed: 12834633]
14. Engel, J., Jr; Van Ness, PC.; Rasmussen, TB.; Ojemann, LM. Outcome with respect to epileptic seizures. In: Engel, J., Jr, editor. Surgical Treatment of the Epilepsies. 2. New York: Raven Press; 1993. p. 609-621.
15. Lin DD, Barker PB, Hatfield LA, Comi AM. Dynamic MR Perfusion and Proton MR Spectroscopic Imaging in Sturge-Weber Syndrome: Correlation With Neurological Symptoms. J Magn Reson Imaging. 2006; 24(2):274–281. [PubMed: 16786573]
16. Oguz KK, Senturk S, Ozturk A, Anlar B, Topcu M, Cilia A. Impact of Recent Seizures on Cerebral Blood Flow in Patients with Sturge-Weber Syndrome: Study of 2 Cases. J Child Neurol. 2007; 22:617. [PubMed: 17690070]
17. Wu Z, Mittal S, Kish K, Yu Y, Hu J, Haacke EM. Identification of calcification with MRI using susceptibility-weighted imaging: a case study. J Magn Reson Imaging. 2009; 29:177–82. [PubMed: 19097156]
18. Yang Q, Liu J, Barnes SR, Wu Z, Li K, Neelavalli J, Hu J, Haacke EM. Imaging the vessel wall in major peripheral arteries using susceptibility-weighted imaging. J Magn Reson Imaging. 2009; 30:357–65. [PubMed: 19629989]
19. Ostergaard L, Weisskoff RM, Chesler DA, Gyldensted C, Rosen BR. High resolution measurement of cerebral blood flow using intravascular tracer bolus passages. Part I: Mathematical approach and statistical analysis. Magn Reson Med. 1996; 36:715–25. [PubMed: 8916022]
20. Ostergaard L, Smith DF, Vestergaard-Poulsen P, et al. High resolution measurement of cerebral blood flow using intravascular tracer bolus passages. Part II: Experimental comparison and preliminary results. Magn Reson Med. 1996; 36:726–736. [PubMed: 8916023]
21. Maria BL, Neufeld JA, Rosainz LC, et al. Central Nervous System Structure and Function in Sturge-Weber Syndrome: Evidence of Neurologic and Radiologic Progression. J Child Neurol. 1998; 13:606–618. [PubMed: 9881531]
22. Lee JS, Asano E, Muzik O, et al. Sturge-Weber syndrome: Correlation between clinical course and FDG PET findings. Neurology. 2001; 57:189–195. [PubMed: 11468301]
23. Evans AL, Widjaja E, Connolly DJA, Griffiths PD. Cerebral Perfusion Abnormalities in Children With Sturge-Weber Syndrome Shown by Dynamic Contrast Bolus Magnetic Resonance Perfusion Imaging. Pediatrics. 2006; 117:2119–2125. [PubMed: 16740855]
24. Reid DE, Maria BL, Drane WE, Quisling RG, Hoang KB. Central Nervous System Perfusion and Metabolism Abnormalities in Sturge-Weber Syndrome. J Child Neurol. 1997; 12:218–222. [PubMed: 9130099]
25. Hendrich KS, Kochanek PM, Melick JA, et al. Cerebral perfusion during anesthesia with fentanyl, isoflurane, or pentobarbital in normal rats studied by arterial spin-labeled MRI. Magn Reson Med. 2001; 46:202–206. [PubMed: 11443729]

26. Chugani HT, Mazziotta JC, Phelps ME. Sturge-weber syndrome: A study of cerebral glucose utilization with positron emission tomography. J Pediatr. 1989; 114:244–253. [PubMed: 2783735]

27. Batista CE, Chugani HT, Juhasz C, Behen ME, Shankaran S. Transient hypermetabolism of the basal ganglia following perinatal hypoxia. Pediatr Neurol. 2007; 36:330–333. [PubMed: 17509466]

28. Wintermark P, Moessinger AC, Gudinchet F, Meuli R. Perfusion-weighted magnetic resonance imaging patterns of hypoxic-ischemic encephalopathy in term neonates. J Magn Reson Imaging. 2008; 28:1019–1025. [PubMed: 18821602]

29. Loeb JA, Sohrab SA, Huq M, Fuerst DR. Brain calcifications induce neurological dysfunction that can be reversed by a bone drug. J Neurol Sci. 2006; 243:77–81. [PubMed: 16430923]

30. Nash TE, Del Brutto OH, Butman JA, et al. Calcific neurocysticercosis and epileptogenesis. Neurology. 2004; 62:1934–1938. [PubMed: 15184592]

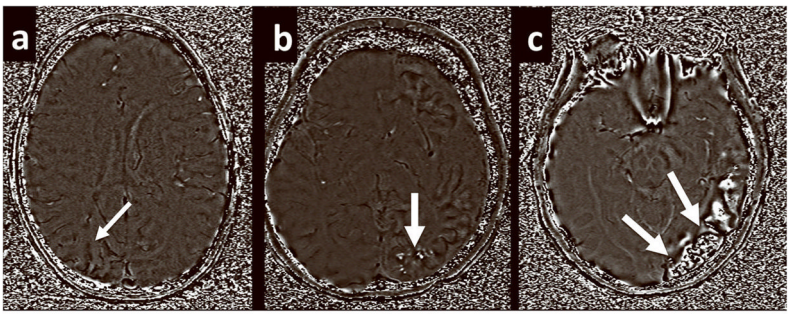

Figure 1.
Examples of how the calcium score was determined based on the phase component images of the SWI data set. (a) A score of 0 was assigned to affected areas without high signal on the phase images. (b) A score of 1 was assigned to areas of punctate foci of high intensity. (c) A score of 2 was assigned to areas of linear hyperintensity.

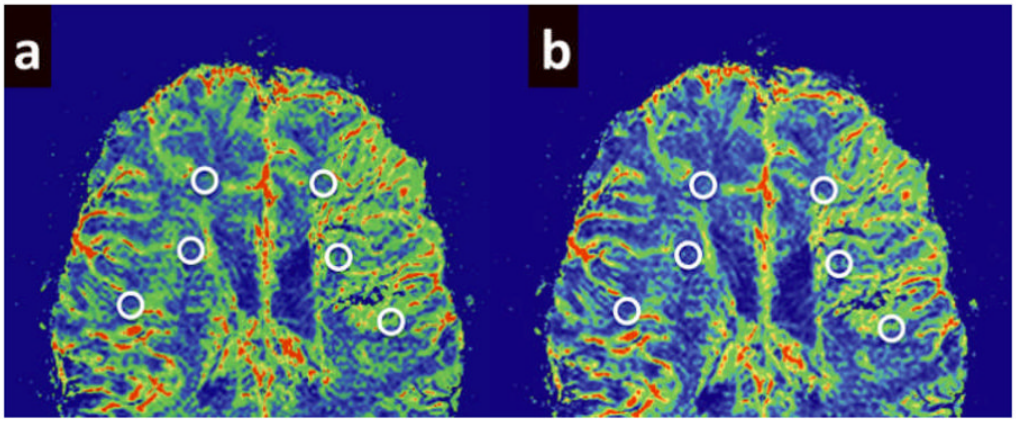

Figure 2.

Examples of ROI placement on the PWI images. ROIs approximately 20–40 voxels in size were placed in white matter beneath affected cortex and in homotopic contralateral cortex. The high resolution PWI images made it relatively easy to identify and avoid placement of ROIs over cortex, ventricle and enlarged transmedullary veins. Measurements were made by two neuroradiologists with a high degree of interobserver concordance. (a) Example of ROI placement on a rCBF image. (b) Example of ROI placement on a rCBV image.

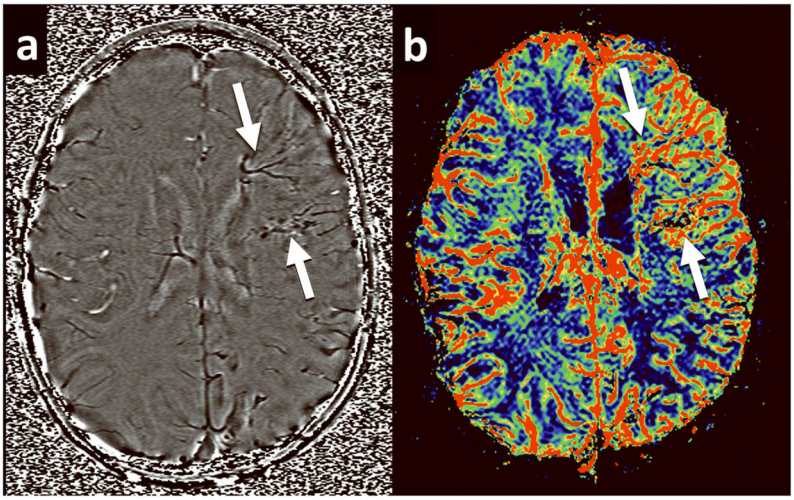

Figure 3.
A 4 year old girl with SWS. (a) Phase image from the SWI acquisition demonstrates dilated transmedullary veins in the white matter beneath the left frontal cortex without areas of increased signal intensity, indicating the lack any calcific deposits. Calcium score = 0 (b) Corresponding rCBF map for the same patient demonstrates increased blood flow in the affected lobe.

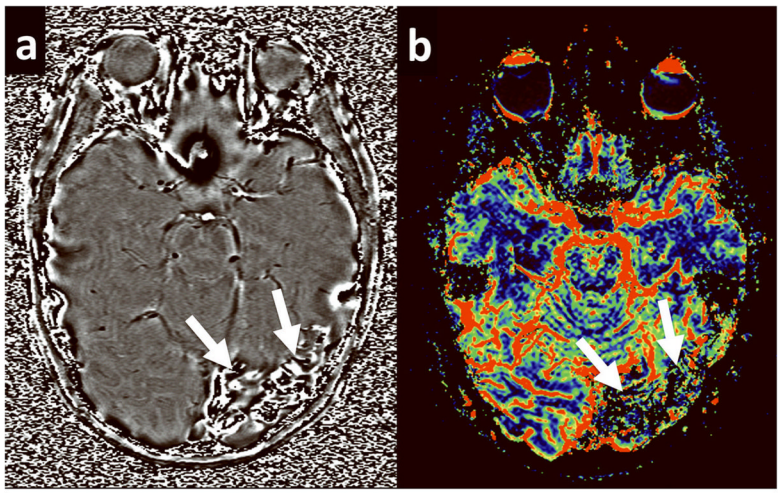

Figure 4.

A 10 year old girl with SWS. (a) Phase image from the SWI acquisition demonstrates linear areas of increased signal signal intensity in the left occipital lobe. Calcification score = 2. (b) Corresponding rCBF map for the same patient demonstrates decreased flow in the corresponding cortex and white matter.

Table 1

Clinical data and calcification scores determined by analysis of susceptibility weighted imaging (SWI)

Patient No.	Gender	Age (yrs)	Age at onset (yrs)	Epilepsy duration (yrs)	Seizure frequency score	Seizure burden score	Angioma side	Lobe of calcification	Calcif. Score
1	M	7	0.5	6.5	6	39	left	FPO	2
2	F	2	0.1	1.9	2	3.8	left	FPO	2
3	F	10	0.2	9.8	4	39.2	left	FPO	2
4	F	5	0.5	4.5	1	4.5	left	TO	2
5	M	5	4.5	0.5	4	2	right	---	0
6	M	1.8	0.8	1	5	5	left	PTO	2
7	F	0.9	0.3	0.6	4	2.4	right	O	1
8	M	4	3.5	0.5	5	2.5	left	---	0
9	M	9	0.6	8.4	2	16.8	left	----	0
10	F	1.6	0.6	1	3	3	right	----	0
11	M	1.8	1.6	0.2	3	0.6	right	O	1
12	F	2	na	0	0	0	left	---	0
13	F	4	2	2	1	2	left	---	0
14	F	4	0	4	1	4	left	----	0
15	F	8	4.5	3.5	1	3.5	right	----	0

F: frontal lobe, P: parietal lobe, T: temporal lobe, O: occipital lobe. Seizure burden score: (duration × seizure frequency score)

Table 2

. White matter perfusion values and asymmetry indices (AIs) ipsi- (I) and contralateral (C) to the leptomeningeal angioma

Patient No.	rCBF-AI	rCBF-I (ml/100g/min)	rCBF-C (ml/100g/min)	rCBV-AI	rCBFV-I (ml/100g)	rCBV-C (ml/100g)	rMTT-AI	rMTT-I (s)	rMTT-C (s)
1	−0.82	16.65	39.67	−0.67	2.33	4.65	−0.44	4.58	7.17
2	−0.28	44.49	58.84	−0.13	4.77	5.41	−0.02	5.65	5.75
3	−0.67	29.04	58.42	−0.52	3.33	5.68	−0.53	3.46	5.95
4	−0.39	22.16	32.87	−0.33	3.49	4.88	−0.19	7.48	9.02
5	−0.16	35.08	41.26	0.02	3.96	3.87	0.27	7.46	5.67
6	−0.46	30.77	49.03	−0.24	2.31	2.93	−0.99	1.22	3.63
7	−0.19	64.57	77.80	−0.07	5.82	6.27	0.11	5.57	4.99
8	−0.12	50.24	56.56	−0.08	4.88	5.31	0.04	5.91	5.71
9	−0.22	20.17	25.14	0.05	1.08	1.03	0.19	3.19	2.64
10	0.39	63.05	42.52	0.69	6.11	2.97	0.29	5.83	4.36
11	0.32	20.40	14.70	0.31	6.00	4.38	0	17.64	17.57
12	0.26	19.66	15.11	0.24	5.73	4.52	−0.02	17.85	18.14
13	0.3	84.04	62.13	0.41	6.92	4.56	0.12	5.18	4.60
14	0.29	55.03	41.02	0.37	5.21	3.58	0.06	6.00	5.64
15	−0.04	69.14	71.75	−0.1	4.70	5.22	−0.08	4.09	4.43

rCBF: relative cerebral blood flow, rCBV: relative cerebral blood volume, rMTT: relative mean transit time, AI: asymmetry index;